160,000-r/min, 2.7-kW Electric Drive of Supercharger for Automobiles

Toshihiko Noguchi, *Senior Member*, Yosuke Takata
Department of Electric, Electronics, and Information Engineering
Nagaoka University of Technology
1603-1 Kamitomioka, Nagaoka, Niigata 940-2188, Japan
tnoguchi@vos.nagaokaut.ac.jp

Yukio Yamashita, and Seiichi Ibaraki
Nagasaki Research & Development Center
Mitsubishi Heavy Industries, Ltd.
5-717-1 Fukahori, Nagasaki, Nagasaki 851-0392, Japan

***Abstract*—This paper describes an ultra high-speed permanent-magnet synchronous motor drive for a supercharger of an automobile internal combustion engine. Conventional superchargers are mechanically linked to and driven by the engine to compress vaporized fuel/air mixture to the engine cylinder. This mechanical linkage does not allow using a high-speed centrifugal compressor, which features higher efficiency and higher boost pressure than a positive displacement compressor. However, an ultra high-speed electric drive makes it possible to use the centrifugal compressor and to improve total system efficiency and the boost pressure response because of no mechanical linkage to the engine. In addition, higher controllability of the boost pressure can be obtained by the electric drive of the supercharger, combining power electronics with the internal combustion engine system. In this paper, a 160,000-r/min, 2.7-kW permanent-magnet synchronous motor drive is discussed and its experimental test results are presented to show excellent performances of the proposed system.**

Keywords-supercharger; centrifugal compressor; ultra high-speed permanent magnet synchronous motor; pseudo-current-source inverter;

I. INTRODUCTION

Automotive superchargers are mechanically linked to an internal combustion engine with a belt from a crankshaft through overdrive devices and compress the air flow to the engine cylinder with mechanical power provided by the engine. Most of conventional superchargers employ a positive displacement compressor rather than a centrifugal compressor because of the operating speed restricted by the engine rotation. The main drawbacks of the positive displacement compressors are its low-efficiency and low-boost pressure.

Electric drive of the supercharger makes it possible to employ a centrifugal compressor instead of the positive displacement compressor because the rotating speed and torque of the compressor can be controlled independently of the mechanical action of the engine. The electrically driven centrifugal compressor, which is more efficient and provides higher boost pressure, allows eliminating the mechanical linkage with the engine and reducing mechanical power loss of the engine. Even though electric motor and power converter losses are taken into account, sufficient improvement of the total system efficiency is expected.

This paper focuses on an electric drive of the supercharger with an ultra high-speed permanent-magnet synchronous motor (PMSM) and the following technical targets are set:

1) A quick response of the boost pressure within several hundred milliseconds from possible low operating speed up to 140,000 r/min.
2) The maximum rotating speed of 160,000 r/min.
3) Size reduction of the motor and the power converter for easy implementation in automobiles.

In order to overcome the problems to achieve the above goals, a guideline of designing the ultra high-speed motor and the power converter is discussed, and experimental test results are presented, using a developed prototype, in this paper.

II. ULTRA HIGH-SPEED PERMANENT-MAGNET SYNCHRONOUS MOTOR DESIGN

A. Required Specifications

In order to electrify the supercharger with a centrifugal compressor, the following specifications are required to design an ultra high-speed PM motor:

First of all, a load of the motor is assumed to be a centrifugal compressor for a 1.5-2.0-litter gasoline engine. It is required to accelerate the compressor from a low speed at an engine idling state to 140,000 r/min within several hundred seconds, which is almost comparable with a response time of conventional superchargers. In addition to this requirement, 2.0-kW output power is needed to obtain sufficient boost pressure. To satisfy these requirements, double of the output torque is indispensable during the acceleration, which corresponds to the instantaneous maximum power is 4 kW.

TABLE I DESIGN SPECIFICATIONS OF ULTRA HIGH-SPEED PMSM.

Rated power (cont.)	2.0 kW
Rated torque (cont.)	0.136 N/m
Rated speed (cont.)	140,000 r/min
Maximum speed	160,000 r/min
Maximum power	4.0 kW
200-% overload duration	0.5 s

TABLE I lists the design specifications of the ultra high-speed PMSM discussed in this paper.

B. Discussion on Stator Configuration

Two sorts of the stator structure have been discussed in the development process of the ultra high-speed PMSM. One is a three-slot stator and the other is a six-slot stator. Both of them have a same winding scheme and an identical rotor, i.e., concentrating windings and a surface permanent-magnet rotor. Operation characteristics of the both motors are examined through magnetic field analyses and simulations prior to the experimental tests of the drive. Since the maximum operating speed of these motors reaches 160,000 r/min, the number of poles is two and extremely thin electromagnetic steel plates of 0.1-mm thickness are employed to construct a laminated stator iron core, which effectively reduces the stator iron loss. In addition, a wide air gap structure is employed to obtain a sinusoidal magnetromotive force across the air gap, which is possible by mounting a highly strong Sm-Co permanent magnet on the rotor. Furthermore, the wide air gap allows the rotor to be reinforced by an alloy sleeve and/or a carbon fiber against extremely strong centrifugal force.

The number of turns per pole is expressed by the following equation:

$$N = \frac{E}{4.44 k_d k_p \phi_m}, \quad \cdots\cdots (1)$$

where E is an induced voltage per pole, k_d is a distributed winding factor, k_p is a shot pitch coefficient, and ϕ_m is a total magnetic flux. Therefore, the distributed winding factors and the short pitch coefficients of the three-slot and the six-slot machines are derived as follows:

$$k_{d3-slot} = k_{d6-slot} = 1; \quad \cdots\cdots (2)$$

$$k_{p3-slot} = \sin\left(\frac{2}{3}\frac{\pi}{2}\right) = 0.866 \text{ ; and} \quad \cdots\cdots (3)$$

$$k_{p6-slot} = \sin\left(\frac{1}{3}\frac{\pi}{2}\right) = 0.5. \quad \cdots\cdots (4)$$

As shown in the above equations, the number of turns of the three-slot machine is 0.58 times of that of the six-slot one. This fact implies that the space factor of the former is larger than that of the latter, which leads easy implementation of the stator windings and forced air-cooling through the stator slots. This feature matches the mechanical configuration of the supercharger because an air-cooling fan can be mounted on the opposite side of the supercharger compressor. However, there is a great concern about spatial harmonics caused by roughly allocated stator teeth and slots of the three-slot machine. Since permeance of the three-slot machine detrimentally varies with respect to radial direction around the rotor, an eddy current loss possibly appear even on the rotor magnet as well as in the stator iron core. The eddy current loss on the rotor results in considerable temperature rise and fatal demagnetization of the Sm-Co permanent magnet. Therefore, it is absolutely necessary to design the optimum shape of the stator teeth and slots to reduce the spatial variation of the permeance.

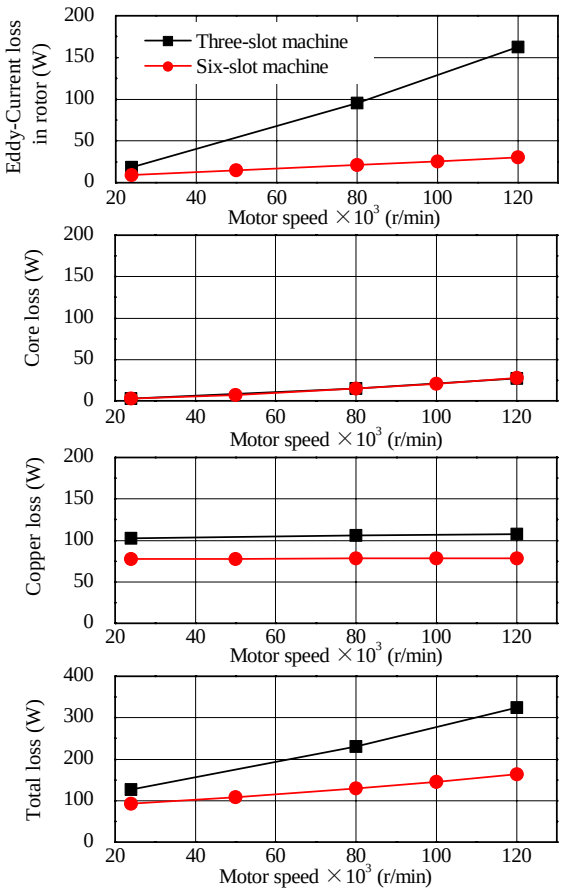

Fig. 1. Loss analysis result of three-slot and six-slot machines.

C. Loss Analysis Results

Loss analyses of the three-slot and the six-slot machines were conducted, using a boundary element method and a finite element method. The boundary element method was applied in the transition part between the stator iron core and the air gap, while the finite element method was used in other else part. Fig. 1 shows loss analysis results of the both machines at 2-kW output power. As can be seen in the figure, the eddy current loss on the rotor magnet differs between the two motors and the three-slot machine dissipates the power 5 times of that of the six-slot machine. This apparent difference is due to the permeance variation of the three-slot machine as described before. From this result, it is found that more than 150 W of the eddy current loss is dissipated in the three-slot machine at 120,000 r/min, which results in the total loss of 300 W. On the other hand, the iron core loss of the stator does not show remarkable difference between the two machines. Therefore, reducing the eddy current loss on the rotor magnet is significant to prevent detrimental temperature rise that leads demagnetization of the permanent magnet. In general, rare earth metal permanent magnet such as Sm-Co is endurable against higher temperature than Nd-Fe-B permanent magnet. Taking thermal conductivity and capacity of the rotor into account, the over 150-W rotor loss possibly raise the rotor temperature over 150 ºC kin the steady state. However, superchargers are required not to rotate continuously but to rotate at high speed mainly during acceleration of the

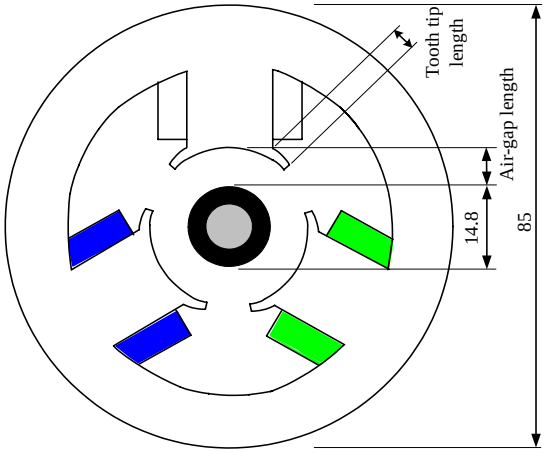

Fig. 2. Principal dimensions of three-slot machine.

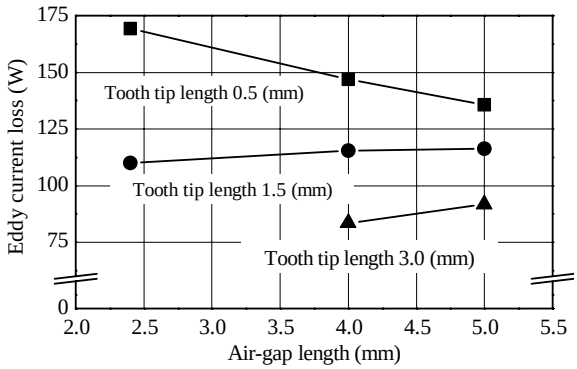

Fig. 3. Eddy current loss at 140,000-r/min and 2-kW operating condition.

automobiles, hence the rotor temperature rise can be limited under a safe operating level.

D. Optimization of Stator Teeth and Slots Shape

In order to reduce the spatial harmonics of the three-slot machine, the shape of the stator teeth and slots was designed as shown in Fig. 2. In other words, semi-closed slots were introduced to the machine to minimize the permeance variation in the direction of rotation. The most important dimensions that influence the eddy current loss are the air-gap length and the slot openings.

Fig. 3 represents a relationship between the eddy current loss on the rotor and the air-gap length at 140,000-r/min and 2-kW operating condition. This graph is depicted, taking a tooth top length (slot opening) as a parameter. As can be found in this analytical result, the longer the tooth tip is (the narrower the slot opening is), the more eddy current loss can be reduced regardless of the shorter air-gap length. Since there is a tradeoff between the stator iron core loss and the air-gap length, it is not recommended to shorten the air-gap excessively. Therefore, 3-mm tooth tip and 4-mm air-gap length were adopted to the actual prototype motor design for the supercharger.

Fig. 4 represents an example of magnetic field analysis result at 120,000 r/min and 2-kW output condition, which

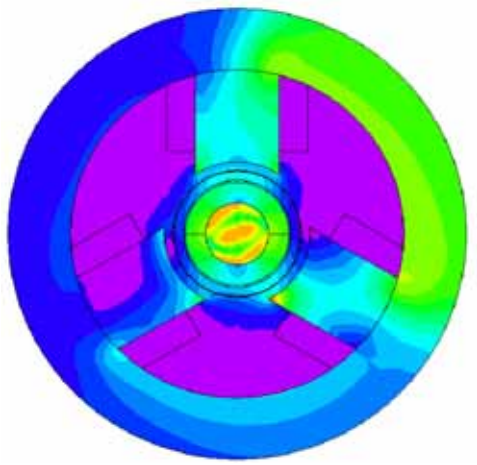

Fig. 4. Flux density distribution of three-slot machine.

indicates flux density distribution of the three-slot machine with no modifications in the stator teeth and slots shape. The flux density in the air-gap is approximately from 0.4 to 0.5 T on average.

III. Pseudo-Current Source Inverter Drive for Ultra High-Speed PMSM

In general, a voltage-source PWM inverter is very often used to operate a PMSM, where a vector control scheme is usually adopted in a microcomputer-based controller that requires current minor loops, sinusoidal current regulation, and coordinate transformations. However, the sinusoidal motor current regulation is hardly possible in the case of ultra high-speed drives because the fundamental frequency of the motor currents is several kilo-hertz at the base speed or the maximum operating speed, which does not allow the inverter to perform the pulse width modulation appropriately. The ultra high-speed PMSM for the supercharger described in this paper reaches 2.3 kHz at the maximum rotating speed of 140, 000 r/min. Therefore, a pseudo-current-source inverter shown in Fig. 5 is employed to drive the ultra high-speed PMSM.

This inverter features a special circuit topology that can be divided into two parts, i.e., a current-controlled buck-boost chopper, and a 120-deg conduction 6-step inverter. The current-controlled chopper is a substitute for a combination of a large DC reactor and a phase-controlled thyristor bridge. Since the switching frequency of the MOSFETs S_{C1} and S_{C2} is 48 kHz, the inductance of the DC reactor can dramatically be reduced, which leads size reduction of the reactor. In addition, current controllability and response are considerably improved by the high-switching frequency, compared with the conventional thyristor-based converter. Using the current-controlled buck-boost chopper across the DC bus, the motor current amplitude is regulated by means of a pulse amplitude modulation (PAM) technique by adjusting the chopper duty ratio. When the motor is in a motoring mode, the chopper acts as a buck chopper and can be regarded as a regulated current source from the inverter. However, at every moment of commutation in the inverter, surge voltages appear on the motor terminals due to the winding inductance of the motor. These surge voltages are clamped by the DC bus voltage

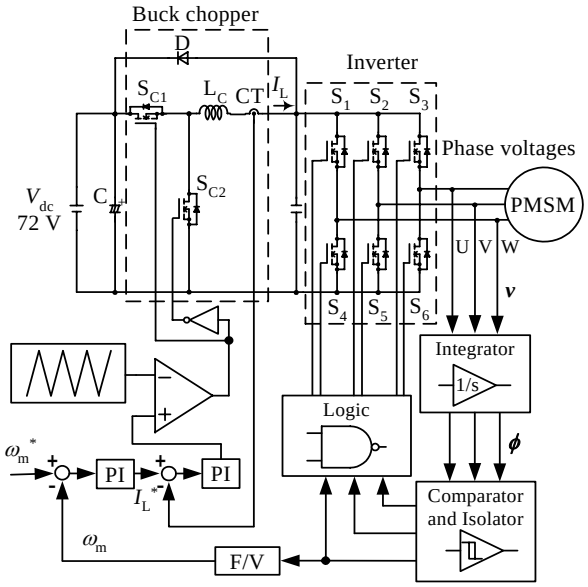

Fig. 5. Schematic diagram of Pseudo-current-source inverter.

through a bypass diode of the chopper and body diodes in the MOSFETs of the inverter. Therefore, it is not necessary to implement blocking diodes in series with the inverter switching devices and the power source of the inverter can be regarded as a voltage source just during the commutation rather than the chopper-controlled current source.

On the other hand, the 6-step inverter with 120-deg conduction period controls the frequency and the relative phase of the motor currents. The commutation of the inverter is carried out on the basis of an e.m.f.-based mechanical sensorless control algorithm of the PMSM. The 120-deg conduction pattern is simply generated by using several analog-and-logic mixed signal circuits, i.e., a motor terminal voltage detector, integrators to calculate the flux linkages, a flux signal isolation circuit composed by photo-couplers and a 120-deg conduction pattern generator. One of the isolated flux signals is used to detect the motor speed and is converted to an analog signal with a F/V conversion circuit. The motor speed controller consists of an ordinary PI element, which provides a current command to the current-controlled buck-boost chopper. As described above, since the mechanical sensorless control algorithm of the system is basically requires detection of the motor back e.m.f., it is impossible to detect the back e.m.f. at a standstill state and is rather difficult to control the motor in a low-speed range. Therefore, open loop control is applied to start up the motor until the operating speed reaches 10,000 r/min. While the open loop control is carried out, the 120-deg conduction pattern is generated with a voltage-controlled oscillator and the conduction pattern generator described before. After reaching the speed threshold of 10,000 r/min, the 120-deg conduction pattern is switched over to that generated by the e.m.f.-based circuit.

IV. Computer Simulations

Several computer simulations were conducted to examine the basic operation performances prior to experimental tests. The test motor has identical specifications as listed in TABLE I

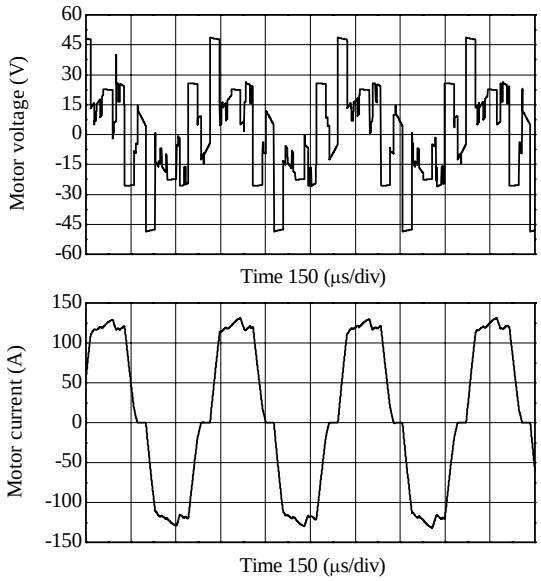

Fig. 6. Motor voltage and current waveforms at 140,000-r/min and 4-kW overload condition (simulation result).

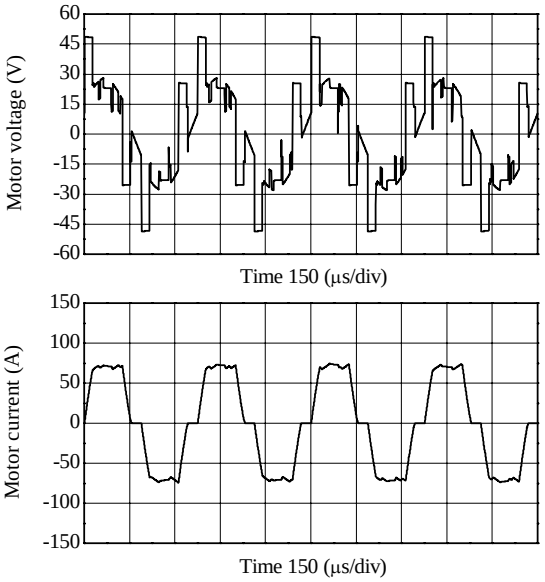

Fig. 7. Motor voltage and current waveforms at 160,000-r/min and 2.7-kW operating condition (simulation result).

and its stator teeth and slots shape is designed to be 3 mm for tooth tip length and 4 mm for air-gap length, respectively. The pseudo-current source inverter has a 72-V DC bus voltage and an 80-μH reactor in the chopper.

Fig. 6 shows a simulation result of the operation at a 140,000-r/min and 4-kW overload condition. As can be seen in this figure, the motor current is properly commutated with a six-step conduction waveform, while the terminal voltage waveform is almost sinusoidal. The surge voltage pulses are observed at every moment of commutation but are clamped by the DC bus voltage. Since the clamped voltage restricts a di/dt rate during the current commutation, the current waveform is similar to a trapezoidal one.

Fig. 8. Photograph of supercharger driven by 160,000-r/min, 2-kW PMSM.

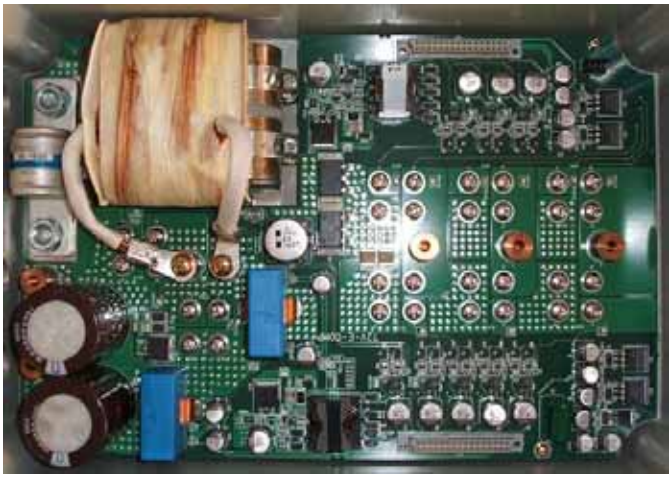

Fig. 9. Photograph of pseudo-current source inverter.

Fig. 7 shows another simulation result of the maximum output operation at the maximum speed of 160,000 r/min. The restricted di/dt rate during the current commutation does not allow the pseudo-current source inverter to output higher peak current and more power to the motor than 75 A and 2.7 kW, respectively. However, overall feasible operations of the proposed system are confirmed by the simulation results presented here.

V. Experimental System Setup and Results

A. Experimental System Setup

A prototype of the ultra high-speed PMSM drive was setup for experimental tests. The drive satisfies the ratings and the specifications listed in TABLE I. Fig. 8 shows a photograph of a test supercharger electrically driven by the 160,000-r/min, 2-kW PMSM. As shown in this photograph, the centrifugal compressor is mounted on one side of the ultra high-speed PMSM, where an air intake is on the left hand side and the compressor exhausts through a pipe with an orifice and a pressure gauge. A cooling fan is attached on the other side of the motor and inhales the ambient air into the motor. Fig. 9 indicates a photograph of the pseudo-current source inverter. The power circuit is entirely composed on a multi-layer printed circuit board with highly thick copper patterns. This structure allows the inverter to reduce line inductance as well as line resistance, which is essential to drive the ultra high-speed PMSM. In general, since such an ultra high-speed machine as

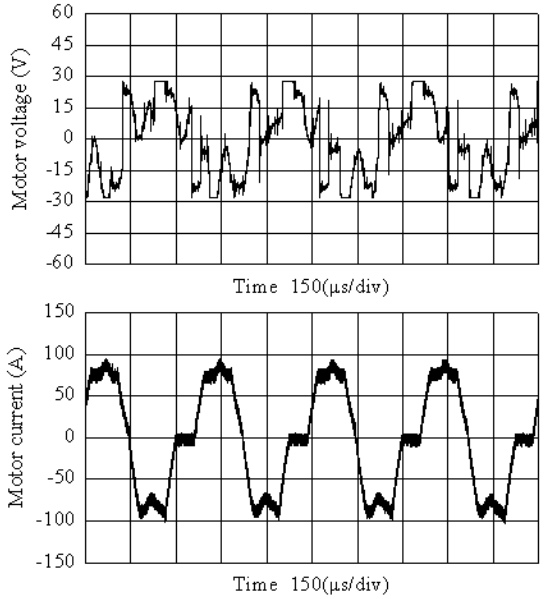

Fig. 10. Motor voltage and current waveforms at 160,000-r/min, 2.7-kW operating condition (experimental result).

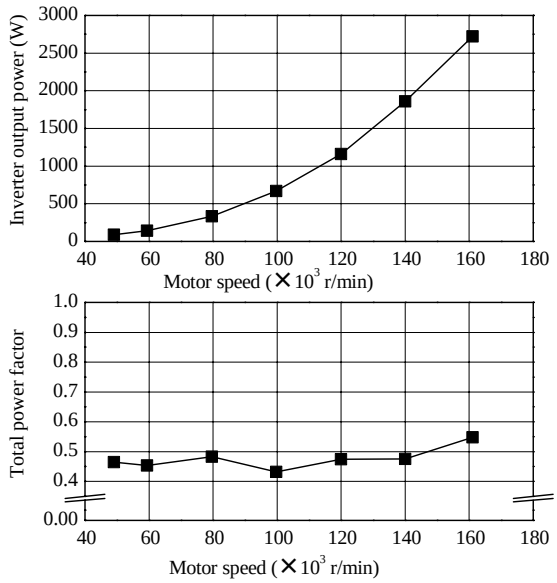

Fig. 11. Inverter output power and total power factor (experimental result).

described in this paper has an extremely low winding inductance, e.g., less than 10 μH, it is significant and indispensable to reduce the line inductance in the inverter as low as possible. In order to reduce the line impedance, In the prototype, MOSFETs with 60-V and 150-A ratings are employed and two of them are operated at 48-kHz in the buck-boost chopper. Also, the DC bus reactor has a same inductance value as that assumed in the simulations.

B. Operating Waveforms and Static Characteristics

Fig. 10 shows voltage and current waveforms of the prototype ultra high-speed PMSM. The operating speed and the output power are 160,000 r/min and 2.7 kW, which is identical with the simulation condition depicted in Fig. 7. As

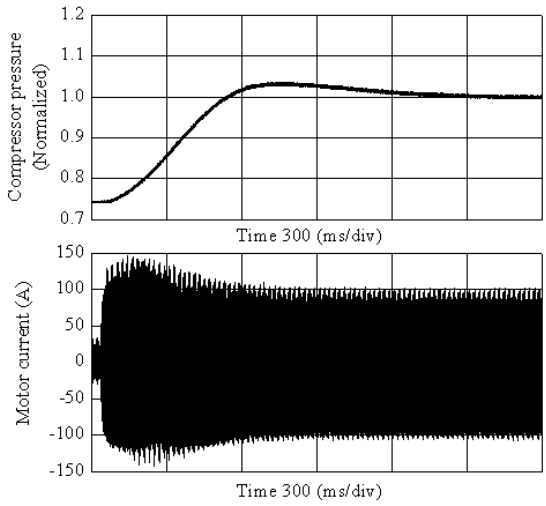

Fig. 12. Transient response of compressor pressure and motor current (experimental result).

can be seen in this figure, the 120-deg conduction pattern of the motor current is distorted due to an improper pattern generation of the controller. One of the reasons for the improper pattern generation is the surge voltage during current commutation, which prevents accurate calculation of the flux linkages. Another reason is impedance drop of the stator windings, which causes a relative phase error of the 120-deg conduction pattern with respect to the back e.m.f. Fig. 11 represents the inverter output power and the total power factor. Since the load of the motor is a centrifugal compressor, which is a typical fluid mechanism, the output power increases as a cubic polynomial function of the rotating speed. On the other hand, the total power factor is around 0.5 regardless of the operating speed or the output power. As pointed out before, the total power factor is hard to improve because the 120-deg conduction waveform inherently includes a large amount of harmonics and is detrimentally affected by the impedance drop of the stator windings. Therefore, compensation of the impedance drop must be investigated to improve the total power factor in the future work.

C. Dynamic Response of Supercharger

Fig. 12 shows a dynamic response of supercharger electrically driven by the prototype PMSM. The figure depicts compressor boost pressure when the speed command is changed stepwise from 50,000 r/min to 140,000 r/min, where the vertical axis is normalized with a target value of the boost pressure. Although the response can be changed by adjusting the PI gain of the speed regulator, higher gain to obtain a faster response makes the mechanical sensorless control unstable. Therefore, the PI gain was experimentally adjusted not to make the system unstable but to achieve the fastest response in the boost pressure. As can be seen in this figure, the response time of the boost pressure is approximately 0.5 s and this result surpasses that of the conventional superchargers.

VI. CONCLUSION

This paper described an ultra high-speed permanent magnet synchronous motor drive applied to automobile superchargers. Particularly, the paper focused on a guideline to design the motor, using a magnetic field analysis based on boundary and finite element methods. In addition to the above theoretical aspect, a three-slot machine prototype was set up to verify experimentally the operation performances and basic characteristics of the drive are examined through experimental tests as well as computer simulations.

According to the magnetic field analysis result, an optimum shape of the stator teeth and slots was designed to reduce an eddy current loss on the rotor magnet. Furthermore, controllability of the ultra high-speed PMSM with a pseudo-current source inverter was verified through computer simulations. Every simulation result proved excellent operating characteristics of the proposed system. However, experimental result pointed out some problems on current waveform generation at a higher current and more power condition. In such an experimental situation, the 120-deg conduction pattern is detrimentally distorted due to the simplified mechanical sensorless control algorithm; hence it is necessary to improve the algorithm in the future work.

However, the paper demonstrated a continuous operation of the drive at 160,000-r/min speed and 2.7-kW output and confirmed an excellent response of the boost pressure with the prototype supercharger, i.e., 0.5 s. Every result proves feasibility of the proposed system and indicates possibility of the electrification of the automobile supercharger.

REFERENCES

[1] Bon-Ho Bae, and Seung-Ki Sul, “A Compensation Method for Time Delay of Full-Digital Synchronous Frame Current Regulator of PWM AC Drives,” *IEEE Trans. on Industry Applications*, vol. 39, no. 3, p.p. 802-810, 2003.

[2] Bon-Ho Bae, Seung-Ki Sul, Jeong-Hyeck Kwon, and Ji-Seob Byeon, “Implementation of Sensorless Vector Control for Super-High-Speed PMSM of Turbo-Compressor,” *IEEE Trans. on Industry Applications*, vol. 39, no. 3, p.p. 811-818, 2003.

[3] Koichi Shigematsu, Jun Oyama, Tusyoshi Higuchi, Takashi Abe, and Yasuhiro Ueno, "The Novel Approach of Coupled Analysis for Small Size and Ultra-High Speed Motor," *IEE-Japan Proc. IAS Annual Conference*, no85, p.p. 349-352, 2003 (in Japanese).

[4] Mitsukichi Okawa, "Design Manual of Magnetic Circuit and PM Motor," Sogo Research, 1989 (in Japanese).

[5] Takehisa Koganezawa, Isao Takahashi, and Kazunobu Oyama, "Sensorless Speed Control of a PM Motor by a Quasi-Current Source Inverter," *IEE-Japan Proc. IAS Annual Conference*, p. 175, 1992 (in Japanese).

[6] Isao Takahashi, Takehisa Koganezawa, T. Su G., and Kazunobu Ohyama, “A Super High Speed PM Motor Drive System by a Quasi-Current Source Inverter.” *IEEE Trans. on Industry Applications*, vol. 30, no. 3, p.p. 683-690, 1994.

[7] Yosuke Takata, Toshihiko Noguchi, Yukio Yamashita, Yoshimi Komatsu, and Seiichi Ibaraki, "220000r/min, 2-kW PM Motor Drive for Turbocharger", *IEE-Japan Proc. IAS Annual Conference*, no. 9, p.p. 155-160, 2004 (in Japanese).

[8] Toshihiko Noguchi, Yosuke Takata, Yukio Yamashita, Yoshimi Komatsu, and Seiichi Ibaraki, "220000r/min, 2-kW Permanent Magnet Motor Drive for Turbocharger", *IEE-Japan International Power Electronics Conference-Niigata*, p.p. 2280-2285, 2005.

[9] Toshihiko Noguchi, Yosuke Takata, Yukio Yamashita, Yoshimi Komatsu, and Seiichi Ibaraki, , "220000r/min, 2-kW PM Motor Drive for Turbocharger", *IEE-Japan Trans. on Industry Applications*, vol. 125, no. 9, p.p. 854-861, 2005 (in Japanese).